Journal of
Synchrotron Radiation

ISSN 1600-5775

Received 30 September 2014
Accepted 31 December 2014

^{57}Fe polarization-dependent synchrotron Mössbauer spectroscopy using a diamond phase plate and an iron borate nuclear Bragg monochromator

Takaya Mitsui,[a]* Yasuhiko Imai,[b] Ryo Masuda,[c] Makoto Seto[a,c] and Ko Mibu[d]

[a]Japan Atomic Energy Agency, 1-1-1 Kouto, Sayo-cho, Sayo-gun, Hyogo 679-5148, Japan, [b]Japan Synchrotron Radiation Research Institute, 1-1-1 Kouto, Sayo-cho, Sayo-gun, Hyogo 679-5198, Japan, [c]Research Reactor Institute, Kyoto University, Kumatori, Sennan-gun, Osaka 590-0494, Japan, and [d]Nagoya Institute of Technology, Gokiso-cho, Showa-ku, Nagoya, Aichi 466-8555, Japan. *E-mail: taka@spring8.or.jp

Energy-domain ^{57}Fe polarization-dependent synchrotron radiation Mössbauer spectroscopy was developed by using a diamond X-ray phase plate and an iron borate nuclear Bragg monochromator. The former controls the polarization of the incident synchrotron radiation X-rays and the latter filters the ^{57}Fe-Mössbauer radiation with a narrow bandwidth of $\sim$3.4 Γ_0 ($\Gamma_0 \simeq 4.7$ neV: natural linewidth of the ^{57}Fe nucleus) from the broadband synchrotron radiation. The developed nuclear diffraction optics allowed ^{57}Fe-Mössbauer studies to be performed with various polarization states, *i.e.* linear polarization, circular polarization and non-polarization. In this paper, the spectrometer system, beam characterization, performance-test experiments and a grazing-incidence Mössbauer measurement of an isotope-enriched (^{57}Fe: 95%) iron thin film are described.

Keywords: Mössbauer spectroscopy; diamond phase plate; nuclear Bragg reflection; nuclear monochromator; polarization analysis; circular dichroism; grazing incidence.

© 2015 International Union of Crystallography

1. Introduction

Mössbauer spectroscopy is a nuclear analytical technique based on the resonant recoil-free absorption and emission of γ-radiation by atomic nuclei bound in a solid, *i.e.* the Mössbauer effect (Mössbauer, 1958). The Mössbauer effect has been observed in approximately 100 nuclides of almost 50 elements. In particular, the most extensively studied isotope in Mössbauer spectroscopy is ^{57}Fe. ^{57}Fe-Mössbauer spectroscopy is a well established method for studying various iron-containing materials. Information on the local magnetic state, valence, electron density and electronic state anisotropy can be obtained through hyperfine interactions between the resonant nucleus and the surrounding electrons. In principle, the nuclear transition probability depends on the direction of the hyperfine magnetic field ($H_{\rm hf}$) and the electronic field gradient at the resonant nucleus with respect to the polarization and the propagation vector of the incoming radiation. Hence, the Mössbauer studies using polarized radiation yield information not or barely obtainable using non-polarized radiation. For example, ^{57}Fe polarization-dependent Mössbauer spectroscopy allows a quick determination of the direction of $H_{\rm hf}$ at ^{57}Fe nuclei and gives a remarkable simplification of the spectral profile. The first study was conducted with a multi-line source (Frauenfelder *et al.*, 1962). However, it is apparent that a well polarized single-line source is desirable to perform the Mössbauer study (Shtrikman, 1967; Shtrikman & Somekh, 1969). A large amount of work has already been undertaken to produce linearly or circularly polarized single-line ^{57}Fe-Mössbauer radiation, and a detailed review covering work up to 2006 has been given by Szymański (2006).

To perform a polarized ^{57}Fe-Mössbauer study, we can generally use two different photon sources, *i.e.* a conventional radioactive ^{57}Co source and a synchrotron radiation (SR) source. In the radioactive ^{57}Co source, the linearly or circularly polarized single-line ^{57}Fe-Mössbauer radiation is obtained by a filtering technique (Szymański *et al.*, 1996; Jäschke *et al.*, 1999); well polarized Mössbauer radiation is separated from allowed nuclear transitions by tuning the resonant velocity condition between the source and the absorber (polarizer). This technique can be easily implemented in laboratories. On the other hand, the strong SR source is the most suitable for performing practical and advanced polarized Mössbauer studies; the excellent beam properties of a well linearly polarized SR source (high brilliance, small beam size, short pulse, *etc.*) enable various applications for polarization-dependent Mössbauer spectroscopy in transmission and scat-

tering geometry. Moreover, one can use a diamond phase plate to control the polarization state of SR X-rays (L'abbé *et al.*, 2004).

The use of a SR source for studying Mössbauer spectroscopy was proposed by Ruby (1974). Since then, a large number of experiments have been performed using a SR source. Generally, there are two kinds of measurement scheme for SR-based Mössbauer spectroscopy. One is the time-domain measurement using nuclear forward scattering (Hastings *et al.*, 1991) and the other is the energy-domain measurement (Odeurs *et al.*, 1998; L'abbé *et al.*, 2000, 2001; Callens *et al.*, 2002; Seto *et al.*, 2009). In the former case a spectrum is recorded as a function of the time after the nuclear excitation by a short resonant synchrotron pulse. The hyperfine parameters are determined by analysis of the quantum beats, whose frequencies are characteristic of the hyperfine structure. Currently, this method is the most established measurement technique (see, for example, Gerdau & van Bürck, 1994; Smirnov, 1996). On the other hand, in the latter case, the nuclear ensemble in both an investigated sample and an oscillating single-line reference sample is collectively excited by the SR pulse. The delayed nuclear resonant scattering is recorded as a function of the velocity of the reference sample so that the energy-resolved spectrum is obtained (stroboscopic detection method). The scattering processes and the information extracted from the spectrum were critically compared between time-domain and energy-domain Mössbauer spectroscopy by Planckaert *et al.* (2009). Note that one can also use an 'exo-interferometric' phase determination method, which enables reconstruction of the energy spectrum from the time-domain measurement (Sturhahn *et al.*, 2004; Callens *et al.*, 2005, 2007). However, the above-mentioned methods depend on the bunch operation modes of SR. It will considerably decrease the overall synchrotron beam time available for SR users. In particular, time-domain measurements require special bunch modes of SR having a rather long period ($T > 100$ ns for ^{57}Fe nuclei) between electron bunches in the storage ring. Unfortunately, such bunch modes are usually limited in SR facilities. Moreover, the energy-domain spectrum, obtained by the stroboscopic detection method, is strongly influenced by the finite experimental time window so that the data analysis is often difficult for users of conventional Mössbauer spectroscopy. However, as for the study of iron-containing materials, the SR user can perform conventional Mössbauer spectroscopy using almost perfect linearly polarized ^{57}Fe-Mössbauer radiation, which is filtered directly from a SR source by a nuclear Bragg monochromator. This method is operational in any bunch mode of SR, which leads to a dramatic increase in the available SR beam time. The principle is based on the nuclear Bragg reflection under the electrically forbidden condition of a single-crystal, which is due to the polarization dependence of nuclear resonance scattering in the presence of a hyperfine interaction (Trammell, 1961; Belyakov & Aivazyan, 1968, 1969; Smirnov *et al.*, 1969; Mirzababaev *et al.*, 1971). The so-called pure nuclear Bragg reflection from a ^{57}Fe-enriched crystal achieves an extremely high suppression of electronic scattering and filters ^{57}Fe-Mössbauer radiation from the SR source. An attempt at this type of measurement was started by Gerdau (Gerdau *et al.*, 1985; Gerdau & Rüffer, 1986). Their experiment successfully showed a Mössbauer spectrum of a diffracted beam from an yttrium iron garnet crystal, using a stainless steel absorber as the analyzer in the energy domain. The theoretical aspects were also discussed by Belyakov (1987*a*,*b*). A breakthrough study of this method was performed by Smirnov *et al.* (1986). Their experiment clearly showed that a pure nuclear Bragg reflection of the $^{57}FeBO_3$ crystal heated up to the Néel temperature in an external field could yield single-line 14.4 keV diffracted γ-radiation with an almost natural linewidth. The first single-line Mössbauer filtration of SR using a heated $^{57}FeBO_3$ crystal was performed at the European Synchrotron Radiation Facility (ESRF) in Grenoble, France (Chumakov *et al.*, 1990), and finally Smirnov realised energy-domain Mössbauer spectroscopy using single-line ^{57}Fe-SR-Mössbauer radiation (Smirnov *et al.*, 1997; Smirnov, 2000). The spectrum was measured by oscillating a sample along the incident ^{57}Fe-SR-Mössbauer radiation. Later, Doppler-shifted single-line ^{57}Fe-SR-Mössbauer radiation at a fixed beam position was successfully produced by oscillating a heated $^{57}FeBO_3$ crystal in the plane of the crystal surface (Mitsui *et al.*, 2007*a*, 2009; Potapkin *et al.*, 2012). A detailed physical picture of single-line ^{57}Fe-SR-Mössbauer radiation was given by Smirnov *et al.* (2011). The first practical application using linearly polarized ^{57}Fe-SR-Mössbauer radiation was demonstrated by a study of the moment canting in an amorphous alloy (Pankhurst *et al.*, 2001). To improve the polarized ^{57}Fe-SR-Mössbauer studies with a nuclear Bragg monochromator, we have recently developed a nuclear diffraction optics using a diamond phase plate and an iron borate nuclear Bragg monochromator to control the polarization states of the incident SR X-rays and/or the filtered ^{57}Fe-SR-Mössbauer radiation. This spectrometer allows us to perform SR-based ^{57}Fe-Mössbauer spectroscopy using a linearly polarized, a circularly polarized and even a non-polarized probe beam in the energy domain. In this paper we describe the technical details of the spectrometer system, beam characterization and performance-test experiments. As a demonstrative study, we introduce a grazing-incidence experiment to observe the circular dichroism on the specular nuclear resonant reflection from a thin layer of ^{57}Fe.

2. Diamond phase plate for ^{57}Fe-SR-Mössbauer radiation

In the developed device, a 750 µm-thick almost perfect diamond single-crystal has been used as a phase plate. A photograph of the crystal is shown in Fig. 1(*a*).

A diamond phase plate is an optical component to utilize the birefringence taking place in the vicinity of the Bragg condition in a perfect crystal (Hirano *et al.*, 1991, 1995; Giles *et al.*, 1994). The π- and the σ-polarization components of the incident X-rays have different phase velocities when they propagate through the crystal, which introduces a phase shift δ between them. If the diffraction plane is inclined by an angle

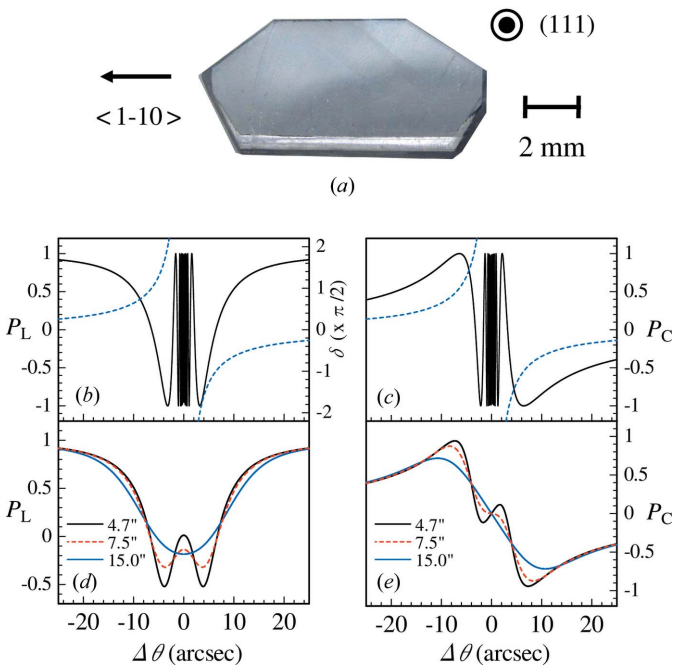

Figure 1
(*a*) Photograph of the diamond single-crystal plate. (*b*, *c*) Solid lines show the calculated angular dependence of degree of linear (P_L) and circular (P_C) polarizations for a perfect plane-wave X-ray at 14.4 keV. Blue dashed lines correspond to the phase difference δ. The phase plate is a 750 µm-thick C (111) crystal, used in the 220 symmetrical Laue case. (*d*, *e*) Calculated angular dependence of P_L and P_C for incident X-rays with three different angular divergences (ω_h = 4.7″, 7.5″ and 15″).

of $\pi/4$ with respect to the electric field of the incident linearly polarized X-rays, the degree of linear polarization, P_L, and circular polarization, P_C, of the transmitted X-rays are proportional to $\cos(\delta)$ and $\sin(\delta)$, respectively. The phase shift δ is given as follows,

$$\delta \approx -\frac{\pi}{2}\left[\frac{r_e^2\,\mathrm{Re}(F_h F_{\bar{h}})}{\pi^2 V^2}\,\frac{\lambda^3 \sin(2\theta_B)}{\Delta\theta}\right] t. \qquad (1)$$

Here, r_e is the classical electron radius, λ is the wavelength, θ_B is the Bragg angle, V is the unit-cell volume, F_h is the structure factor, $\Delta\theta$ is the offset angle and t is the thickness of the crystal. The parameter $\Delta\theta$ is defined as $\Delta\theta = \theta - \theta_B$, where θ is a glancing angle to the net plane. The X-ray transmission rate, T, at an incident angle far away from the Bragg condition is given by

$$T \approx \exp(-\mu t), \qquad (2)$$

where μ is a linear absorption coefficient.

In equation (1) the phase shift is controlled by the offset angle, $\Delta\theta$, from the Bragg condition. Therefore, the crystal setting at $\delta = (n + 1)\pi$ acts as a half-wave plate, so that it rotates a polarization plane of linearly polarized X-rays by 90°. In other cases, the crystal setting at $\delta = (n + 1/2)\pi$ acts as a quarter-wave plate and then the linearly polarized X-rays are converted to circularly polarized X-rays. The phase shift, δ, is calculated for a symmetric C 220 reflection of the perfect plane-wave 100% linearly polarized 14.4 keV X-rays and $t = t_0 / \cos\theta_B$ (t_0 = 750 µm, θ_B = 19.94°), as a function of $\Delta\theta$. Figs. 1(*b*) and 1(*c*) show the theoretical values of P_L and P_C, respectively.

One can see that the phase shift rapidly changes at close proximity to the Bragg condition and slowly changes in the region far away from the Bragg condition. The former case is not suitable for the production of high-quality polarized X-rays. Since, in real experiments, the finite angular divergence of the incident X-rays causes a degradation of the polarization state by way of the spread of δ, the polarization of transmitted X-rays is obtained by convoluting $P_L(\Delta\theta)$ or $P_C(\Delta\theta)$ with an angular distribution of the effective divergence of incident X-rays. In Figs. 1(*b*) and 1(*c*), the theoretical P_L and P_C values near the Bragg condition are extremely sensitive to $\Delta\theta$. As a result, linearly polarized X-rays with finite angular divergence are converted to pseudo non-polarized X-rays (mixed polarization). This indicates that the diamond phase plate close to the Bragg condition works as a depolarizer (Bouchenoire *et al.*, 2003; Ueji *et al.*, 2005). On the other hand, the latter case, which is not sensitive to $\Delta\theta$, is available for precise control of the polarization state of X-rays. Figs. 1(*d*) and 1(*e*) show the calculated angular dependence of P_L and P_C for incident X-rays with three different horizontal angular divergences, ω_h = 4.7″, 7.5″ and 15″. In the calculations we have assumed that the vertical angular divergence, ω_v, is fixed to 3.0″, whose values are comparable with a typical angular divergence of the undulator radiation at SPring-8. In Fig. 1(*d*), as the ω_h value increases from 4.7″ to 15″, P_L degrades rapidly and all calculated values are greater than −0.5. This is because the thickness of 750 µm is not thick enough to act as a half-wave plate for divergent X-rays with energy of 14.4 keV. In contrast, in Fig. 1(*e*), a maximum magnitude on P_C shows a considerably large value ($|P_C|_{max} > 0.85$) for ω_h values less than 7.5″. The X-ray transmission rate, derived from equation (2), is estimated to be about 80%. These values are suitable for a quarter-wave plate: the C 220 phase plate, operating under the off-Bragg condition of $\Delta\theta \sim \pm 8.0''$, can convert the linearly polarized 14.4 keV X-rays with ω_h = 4.7″ to circularly polarized X-rays with $P_C \simeq 0.9$.

3. Optical system and experimental procedure

To perform energy-domain polarized ^{57}Fe-SR-Mössbauer spectroscopy a dedicated optical system has been designed and installed at the BL11XU beamline of SPring-8. It is composed of a high-resolution monochromator, a diamond phase plate and an iron borate nuclear Bragg monochromator. A photograph and a schematic view of the optical set-up are shown in Figs. 2(*a*) and 2(*b*), respectively.

The experimental procedure is as follows. With reference to Fig. 2(*b*), the electron current of the SPring-8 storage ring is kept at 100 mA at 8.0 GeV. A liquid-nitrogen-cooled Si 111 double-crystal monochromator is used to handle the high heat load of undulator radiation (Shiwaku *et al.*, 2004). Linearly σ-polarized (100%) SR X-rays with an energy bandwidth of 2.5 meV at the 14.4 keV nuclear resonance of ^{57}Fe are produced by a nested high-resolution monochromator consisting of asymmetric Si 511 and asymmetric Si 975

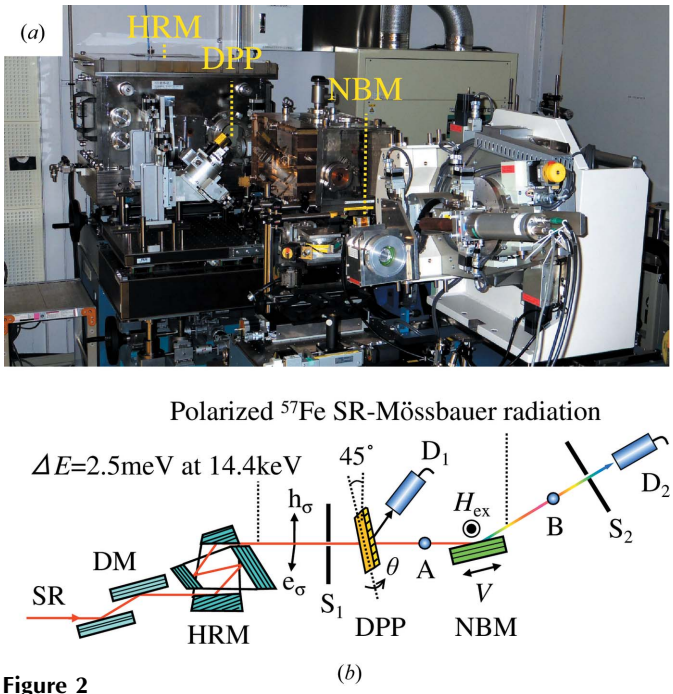

Figure 2
^{57}Fe-SR-Mössbauer spectrometer installed at BL11XU of SPring-8. (*a*) External view and (*b*) nuclear diffraction optical system. SR: synchrotron radiation from the undulator of BL11XU; DM: double-crystal monochromator, Si 111 reflections; HRM: high energy resolution monochromator, nested-type channel-cut Si 511 × Si 975 reflections; S_1: slit 1.0 mm (H) × 1.0 mm (V); DPP: diamond phase plate, C 220 reflection in Laue geometry; D_1: PIN photodetector; NBM: nuclear Bragg monochromator, $^{57}FeBO_3$ 111 reflection near the Néel point; H_{ex}: external magnetic field, 150 Oe; S_2: slit 1.0 mm (H) × 0.5 mm (V); D_2: NaI(Tl) scintillation detector.

channel-cut crystals (Mitsui *et al.*, 2001). The horizontal beam size is restricted by a slit, S_1. Behind S_1 the typical total flux is about 7.5×10^9 photons s^{-1}, the beam size is 1.0 mm (H) × 0.4 mm (V) and horizontal and vertical angular divergences are estimated to be 4.7″ and 3.0″, respectively. The SR X-rays are incident onto the diamond phase plate, adjusting near the symmetric Laue 220 diffraction condition ($\theta_B = 19.94°$). The scattering plane of the phase plate is set to be inclined by 45° from the vertical plane. Then, as described in §2, σ-polarized SR X-rays are converted to circular polarized or non-polarized SR X-rays by changing the parameter $\Delta\theta$ of the phase plate. The polarization-controlled SR X-rays are incident onto a ^{57}Fe-enriched (95%) iron borate nuclear Bragg monochromator, and 14.4 keV ^{57}Fe-SR-Mössbauer radiation is produced by the pure nuclear Bragg reflection of $^{57}FeBO_3$ 111 ($\theta_B = 5.11°$). Here, a static external field of 150 Oe is applied parallel to the crystal surface and perpendicular to the scattering plane to make the hyperfine field parallel to the scattering plane in the 111 plane. Then, the pure nuclear Bragg reflection of $^{57}FeBO_3$ 111 is related to the $\Delta m = \pm 1$ nuclear transitions and its polarization state is in accord with the polarization factor in the nuclear resonance scattering amplitude (van Bürck *et al.*, 1980; Siddons *et al.*, 1989; Smirnov, 2000; Smirnov *et al.*, 2011). In the antiferromagnetic pure nuclear Bragg reflection system of Fig. 2(*b*) the $^{57}FeBO_3$ 111 nuclear Bragg monochromator produces strongly polarized ^{57}Fe-SR-Mössbauer radiation, whose polarization plane is rotated by 90° from that of incident X-rays; the σ-polarized incident SR beam is reflected as π-polarized ^{57}Fe-SR-Mössbauer radiation, while a circularly polarized (or non-polarized) SR beam is reflected as ^{57}Fe-SR-Mössbauer radiation with the same polarization state. Under that condition, the ^{57}Fe-SR-Mössbauer radiation is ultrafinely monochromated by heating the $^{57}FeBO_3$ crystal up to near the Néel point (T_N = 348.8 K), whose energy bandwidth reaches about 3.4 Γ_0 (Mitsui *et al.*, 2007*b*). Here Γ_0 (∼4.7 neV) is the natural linewidth of the ^{57}Fe nucleus. The resonance energy of iron borate is changed by the Doppler effect with the crystal oscillating parallel to the 111 plane in a sinusoidal velocity mode at 10 Hz. Behind S_2 the single-line ^{57}Fe-SR-Mössbauer radiation is counted by a NaI(Tl) scintillation detector. The typical total flux is about 1.0×10^4 photons s^{-1} and the beam size is 1.0 mm (H) × 0.4 mm (V). In Fig. 2(*b*), if a sample is placed at position A or B, the spectrum is obtained by counting the intensity of the pure nuclear Bragg reflection as a function of the velocity. Table 1 summarizes the available polarization states for ^{57}Fe-SR-Mössbauer spectroscopy; the design of the nuclear diffraction optics allows us to perform the ^{57}Fe-Mössbauer studies with various polarization states such as σ/π-linearly polarized, right/left circularly polarized and non-polarized SR X-rays. Here, we adopt a previously reported definition that the right circular polarization corresponds to a positive helicity ($\Delta m = +1$) photon emitted in the direction of H_{hf} at the ^{57}Fe nucleus, where m is the spin quantum number of the photon (Siddons *et al.*, 1999).

Table 1
Available polarization states for ^{57}Fe-SR-Mössbauer spectroscopy.

Polarization state for the incident beam	C 220 phase plate (offset angle)	Position A B
Horizontal linear polarization (σ)	Without	○ ×
Vertical linear polarization (π)	Without	× ○
Circular polarization (right/left)	$\Delta\theta = \pm 8.0''$	○ ○
Non-polarization (mixed polarization)	$\Delta\theta = 0$	○ ○

4. Beam characterization and performance-test experiments

The performance of the developed spectrometer was evaluated in detail. Firstly, to check the quality of the diamond phase plate [behind the HRM in Fig. 2(*b*)], a rocking curve of the C 220 Laue symmetric reflection and the $\Delta\theta$ angle dependence of the P_L value were measured with the 14.4 keV incident SR X-rays. The experimental set-up is shown in Fig. 3(*a*). There are some techniques for the characterization of X-ray polarization (see, for example, Siddons *et al.*, 1989, 1990; Finkelstein *et al.*, 1994; Shen *et al.*, 1995; Shen & Finkelstein, 1995; Shen, 1996, 2000). However, in this study a simple polarimeter was used to measure the P_L value of the SR X-rays; it consisted of a scatterer (polyimide film) and two NaI(Tl) scintillation detectors (Hayakawa *et al.*, 1998; Suzuki, 2004). The detectors D_2 and D_3 counted the vertical (I_y) and horizontal (I_x) components of the scattered X-ray intensities,

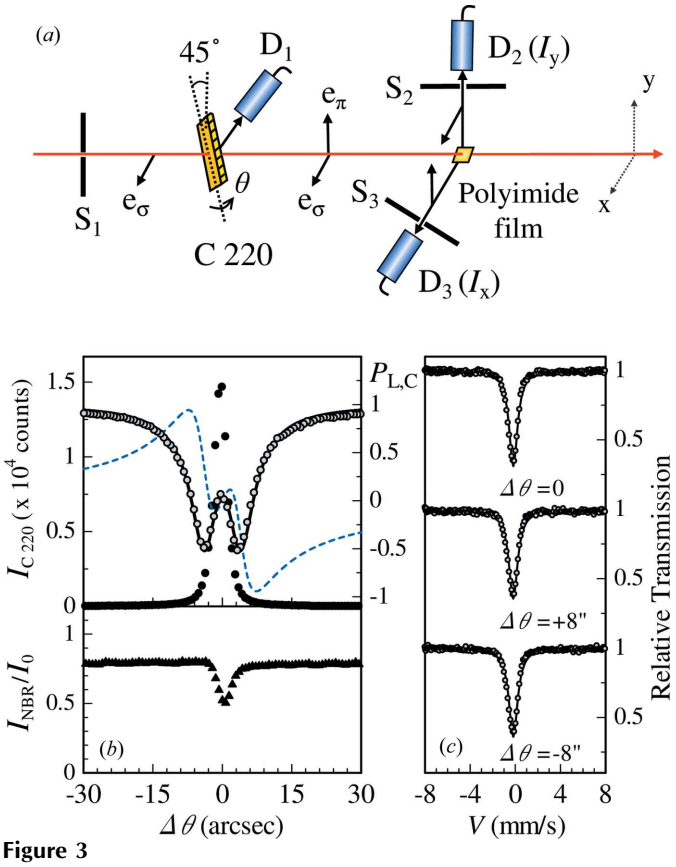

Figure 3
(*a*) Experimental set-up for characterization of the C 220 phase plate. S_1: slit 1.0 mm (H) × 0.5 mm (V); S_2, S_3: slits 1.0 mm (H) × 1.0 mm (V); D_1: PIN photodetectors; D_2, D_3: NaI(Tl) detectors. (*b*) Experimental results. The solid and open circles show a rocking curve of the C 220 reflection and the offset-angle dependence of the measured P_L, respectively. The black solid and blue dashed lines are the theoretical curves of P_L and P_C, respectively. Solid triangles show the offset-angle dependence of the measured peak intensity ratio of the $^{57}FeBO_3$ 111 reflection near the Néel temperature. (*c*) SR Mössbauer absorption spectra of a 2.5 µm-thick stainless steel foil (^{57}Fe 90%) measured at three different offset angles ($\Delta\theta$ = 0, 8.0″ and −8.0″). Solid lines are guides for the eye.

respectively. Because of the polarization dependence of the X-ray scattering, the P_L value was determined by

$$P_L = (I_y - I_x)/(I_y + I_x). \quad (3)$$

The results are shown in the upper part of Fig. 3(*b*). The rocking curve shows a sharp single-peak profile (solid circles) with a narrow full width at half-maximum of 3.65″, whose value is in good agreement with the theoretical one (3.63″). It implies that the diamond phase plate has an ideal crystal perfection, which enables the precise phase control of the transmitted SR X-rays *via* the offset angle $\Delta\theta$. Indeed, the measured P_L values (open circles) are in good agreement with the theoretical curve (solid line). Hence, as shown in the calculated $\Delta\theta$-angle dependence of the P_C value (dashed line), we can expect that the σ-polarized SR X-rays are converted into the circular polarization at $\Delta\theta = \pm 8$ or the non-polarization condition at $\Delta\theta = 0$.

Secondly, the Bragg peak intensity of $^{57}FeBO_3$ 111, I_{NBR}, was measured by changing the offset angle. The typical intensity was about 8.0×10^3 counts s^{-1} at $\Delta\theta = \pm 8''$ and about 5.0×10^3 counts s^{-1} at $\Delta\theta = 0$. The measured intensity curve (solid inverted triangle) is shown in the lower part of Fig. 3(*b*), which is normalized by a Bragg peak intensity obtained without the phase plate, I_0. For the circular polarization conditions ($\Delta\theta = \pm 8''$), the I_{NBR}/I_0 value is about 0.8, which is in good agreement with the calculated X-ray transmission rate of the 750 µm-thick diamond. On the other hand, for the non-polarization condition ($\Delta\theta = 0$), the I_{NBR}/I_0 value decreases to about 0.5, whose physical origin is due to the anomalous absorption caused by the X-ray dynamical diffraction of an almost perfect diamond crystal (Batterman & Cole, 1964).

Thirdly, the energy bandwidth of the ^{57}Fe-SR-Mössbauer radiation was examined at three different offset-angle conditions ($\Delta\theta = 0$ and $\pm 8''$) by measuring the absorption spectra of a 2.5 µm-thick 90% ^{57}Fe-enriched stainless steel foil placed at position B in Fig. 2(*b*). The measured spectra are shown in Fig. 3(*c*). At a glance, we can see that all the spectra exhibit clear single-line absorption profiles with almost the same energy bandwidth. The results prove that the nuclear Bragg monochromator can filter the Doppler-shifted single-line ^{57}Fe-Mössbauer radiation from broadband SR X-rays with different polarization states.

Finally, we characterized the controlled polarization states of the incident SR X-rays and the reflected ^{57}Fe-SR-Mössbauer radiation. The experiment was performed using the nuclear diffraction optics of Fig. 2(*b*) with and without the C 220 phase plate. The linear polarizations and non-polarization were evaluated from the absorption spectra of a 2 µm-thick 90% ^{57}Fe-enriched iron foil. In both cases the foil was magnetized perpendicular to the scattering plane by applying an external field (H_{ex}) of 5.2 kOe. Then, as is shown in Fig. 4(*a*), H_{hf} at the ^{57}Fe nuclei was aligned antiparallel to H_{ex}. The room-temperature Mössbauer spectra were measured for the iron foil placed at positions A or B in Fig. 2(*b*). The measured spectra are shown in Figs. 4(*c*) and 4(*d*), respectively. In the upper part of Fig. 4(*c*) the spectrum, measured without the phase plate, shows a symmetric spectral profile with four absorption lines (first, third, fourth, sixth) of $\Delta m = \pm 1$ nuclear transitions. This is due to the pure σ-polarization of incident SR X-rays at position A. In contrast, as shown in the upper part of Fig. 4(*d*), the spectrum, measured without the phase plate, shows a symmetric spectral profile with two absorption lines (second, fifth) of $\Delta m = 0$ nuclear transitions. The result clearly shows that the ^{57}Fe-SR-Mössbauer radiation has pure π-polarization at position B (Mitsui *et al.*, 2007*a*). On the other hand, in the lower part of Figs. 4(*c*) and 4(*d*), the spectra, measured with the phase plate at $\Delta\theta = 0$, exhibit a similar spectral profile with six absorption lines. The results prove that the incident SR X-rays and the ^{57}Fe-SR-Mössbauer radiation have the non-polarization state, like a conventional ^{57}Co Mössbauer source. The right and left circular polarizations and their P_C values were evaluated from the absorption spectra of a 15 µm-thick non-enriched iron foil. H_{hf} of the iron foil was arranged as much as possible to be parallel to the beam direction (k); as shown in Fig. 4(*b*), the foil in an external field of 5.2 kOe ($H_{ex} \parallel k$) was magnetized in its plane

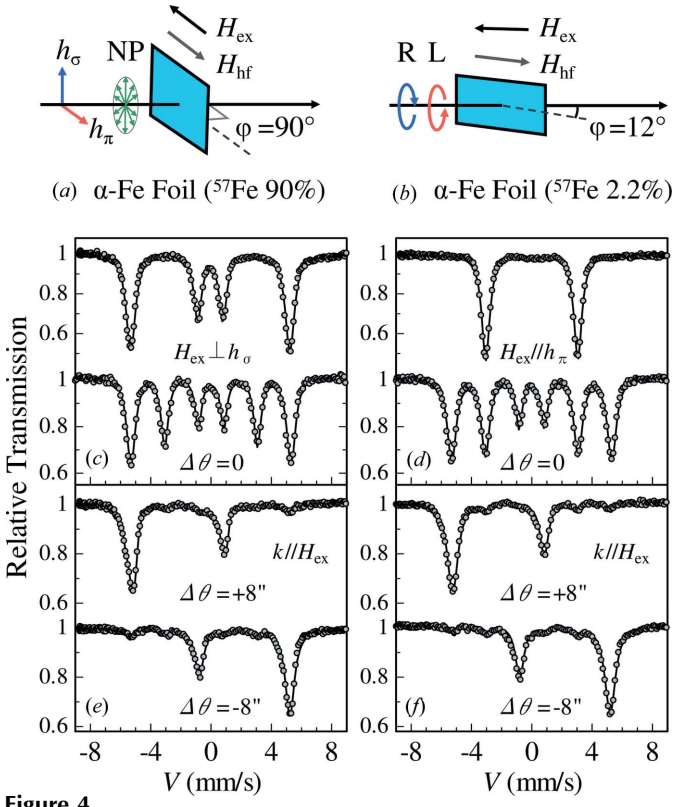

Figure 4
^{57}Fe polarization-dependent SR-Mössbauer spectroscopy of magnetized iron foils. (*a*) Linearly (σ, π) or non-polarized (NP) beams are incident on a 2 µm-thick 90% ^{57}Fe-enriched iron foil, whose H_{hf} is aligned perpendicular to the beam direction and the scattering plane; h_i ($i = \sigma, \pi$) is the magnetic unit vector of the incident beam. (*b*) The circularly (right, left) polarized beam is incident on a 15 µm-thick non-enriched iron foil, whose H_{hf} forms an angle φ (= 12°) with the beam direction. ^{57}Fe-Mössbauer spectra measured for (*c*) σ-polarized and non-polarized SR X-rays at $H_{ex} \perp h_\sigma$, (*d*) π-polarized and non-polarized ^{57}Fe-SR-Mössbauer radiation at $H_{ex} \parallel h_\pi$, (*e*) for right and left circularly polarized SR X-rays at $k \parallel H_{ex}$ and (*f*) right and left circularly polarized ^{57}Fe-SR-Mössbauer radiation at $k \parallel H_{ex}$. Solid lines correspond to calculation. Note that the spectra are measured for the iron foil placed before (*c*, *e*) and after (*d*, *f*) the nuclear Bragg monochromator.

so that H_{hf} was aligned almost parallel ($\varphi = 12°$) to the beam direction, because it is usually difficult to magnetically polarize an iron foil perpendicular to the foil plane. In Fig. 2(*b*) the offset angle of the phase plate was adjusted to circular polarization conditions ($\Delta\theta = \pm 8''$) and the room-temperature Mössbauer spectra were measured for the iron foil placed at position A or B. The results are shown in Figs. 4(*e*) and 4(*f*), respectively. In the upper part of Figs. 4(*e*) and 4(*f*) the spectra, measured with the phase plate at $\Delta\theta = +8''$, show almost the same asymmetric profile with two main absorption lines (first, fourth) of $\Delta m = +1$ nuclear transitions. The results provide clear evidence that the incident SR X-rays and the ^{57}Fe-SR-Mössbauer radiation have right circular polarization. Note that the traces of the other lines (second, third, fifth, sixth) come from incomplete polarization and incomplete alignment of H_{hf} in the iron foil. As discussed in §2, one can switch the helicity of the circularly polarized incident beam by offset-angle reversal. Indeed, as shown in the lower part of Figs. 4(*e*) and 4(*f*), the spectra, measured with the phase plate at $\Delta\theta = -8''$, exhibit the reversed asymmetric profile with two main absorption lines (third, sixth) of $\Delta m = -1$ nuclear transitions. The results prove that the incident SR X-rays and the ^{57}Fe-SR-Mössbauer radiation have left circular polarization.

The P_C values of the incident beam were determined by a fit of the spectra. The theoretical treatment has been described by Szymański *et al.* (1996): in the case of incomplete polarization, the spectrum can be fitted with a linear combination of the functions $N_R S_R(\varphi) + N_L S_L(\varphi)$, where $S_R(\varphi)$ and $S_L(\varphi)$ are the spectra measured with complete right and left circular polarization, φ is the angle between the ^{57}Fe nuclear moment and the beam direction, N_R and N_L are proportional to the number of photons for each polarization. Figs. 4(*e*) and 4(*f*) show the results of curve fitting (solid lines) calculated in the same manner as previously reported (Szymański *et al.*, 1996). From the estimated coefficients N_R and N_L we have determined the degree of right and left circular polarization, $P_C = (N_R - N_L)/(N_R + N_L)$, to be about ± 0.91, in good agreement with the theoretical values as expected in §2.

In this performance-test study the experimental results have clearly demonstrated that the developed spectrometer allows us to perform conventional energy-domain Mössbauer spectroscopy using a polarization-controlled SR probe beam. Certainly, this device can realise the advanced polarization-dependent ^{57}Fe-SR-Mössbauer experiments, which was impossible before. However, the user should note that the energy bandwidth of ^{57}Fe-SR-Mössbauer radiation is still several times larger than that of a radioactive ^{57}Co source. We think that this problem should be improved in future studies.

5. Grazing-incidence experiment with circularly polarized ^{57}Fe-SR-Mössbauer radiation

High-brilliance SR is extremely suitable for grazing-incidence Mössbauer spectroscopy, which is an effective tool for investigation of hyperfine interactions near the surface (see, for example, Bernstein & Campbell, 1963; Wagner, 1968; Frost *et al.*, 1985; Andreeva *et al.*, 1991, 1994; Irkaev *et al.*, 1993). In the early SR-based Mössbauer studies, grazing-incidence anti-reflection (GIAR) multilayer films were intensively studied with regard to the principle of nuclear resonant filtering of SR (Hannon *et al.*, 1979, 1985*a*,*b*,*c*,*d*; Gerdau *et al.*, 1990; Andreeva *et al.*, 1991). Since then, a number of thin film and multilayer systems have been studied by the time-domain measurement (see, for example, Röhlsberger *et al.*, 1993; Chumakov *et al.*, 1993, 1999; Toellner *et al.*, 1995; Niesen *et al.*, 1998; Nagy *et al.*, 1999, 2000; Röhlsberger *et al.*, 2001). The optical properties of a thin film containing a Mössbauer isotope and selected applications have been reviewed by Röhlsberger (1999). Subsequently, the energy-domain measurement of a thin film under grazing-incidence conditions was also performed using the stroboscopic detection method (Bottyán *et al.*, 2003; Deák *et al.*, 2006). These methods are complementary, having their own features and advantages. At present, Mössbauer spectroscopy with single-line ^{57}Fe-SR-Mössbauer radiation is also a potential candidate for devel-

oping the grazing-incidence studies (Mitsui *et al.*, 2012*a*; Potapkin *et al.*, 2012; Mibu *et al.*, 2013). Generally, SR-based grazing-incidence Mössbauer spectroscopy has been performed with a linearly polarized beam. However, a previous work (L'abbé *et al.*, 2004) has demonstrated that the circularly polarized beam is useful for a layer-selective magnetization measurement of a magnetic thin film. Therefore, as a pilot study, we performed a grazing-incidence experiment with circularly polarized ^{57}Fe-SR-Mössbauer radiation to observe the dichroism effect (Gonser & Fischer, 1981, 1985) of the specular nuclear resonant reflection from a thin layer of ^{57}Fe. In this experiment we prepared a 100 nm-thick 95% ^{57}Fe-enriched iron thin film, which was grown using an MBE machine on an MgO(001) substrate. The sample had dimensions of 5 × 30 × 0.5 mm (width × length × thickness).

The experimental set-up is shown in Fig. 5(*a*). The iron thin film, ^{57}Fe(100 nm)/MgO(001), was placed behind the $^{57}FeBO_3$ 111 nuclear Bragg monochromator. The magnetic moment (hyperfine field) was aligned antiparallel (parallel) to the beam direction by applying an external magnetic field (H_{ex} = 600 Oe) in the film plane. Note that an epitaxial Fe/MgO(001) film was magnetically saturated by a weak external field of several hundred Oe in the film plane (Zhan *et al.*, 2009). The room-temperature specular nuclear resonant reflection spectra were measured at a low grazing angle condition of 0.3°. Then the ^{57}Fe-enriched iron thin film acted as a GIAR film: the electron scattering was sufficiently suppressed and only the nuclear resonant scattering contributed to the specular reflection because the critical angle of the nuclear resonant scattering was greater than that of the electron scattering (φ_e = 0.22°). As a result, the specular nuclear resonant reflection occurred when the energy of the incident beam was close to the allowed nuclear transition's resonant energy of the ^{57}Fe nuclei (Isaenko *et al.*, 1994). The X-ray background level was reduced by a restrictive slit (S) in front of a NaI(Tl) detector (D). The spectrum was measured with non-polarized ($\Delta\theta = 0$) and right ($\Delta\theta = +8''$) circularly polarized ^{57}Fe-SR-Mössbauer radiation. In both cases a statistically sufficient spectrum was obtained with a short measurement time of 15 min. Fig. 5(*b*) shows the signal-to-background ratios (SBR) of the measured specular reflectivity spectra. In the upper part of Fig. 5(*b*) the spectrum, measured in the non-polarization state, shows a symmetric spectral profile with four resonance peaks of $\Delta m = \pm 1$ nuclear transitions. The result means that the net magnetization of the iron thin film is sufficiently saturated by a H_{ex} of 600 Oe. In contrast, as shown in the lower part of Fig. 5(*b*), the spectrum, measured with right circular polarization, clearly shows an asymmetric spectral profile with two main resonance peaks of $\Delta m = +1$ nuclear transitions. The result proves that the magnetic moment (hyperfine field) of ^{57}Fe in the thin film is aligned antiparallel (parallel) to the beam direction. As a remarkable effect, it shows a large enhancement in the SBR, whose value is almost twice as large as that of the non-polarized beam incidence case. This result gives clear evidence of circular dichroism on the specular nuclear resonant reflection from a thin layer of ^{57}Fe: in Fig. 5(*a*) the right circularly polarized beam excites only the

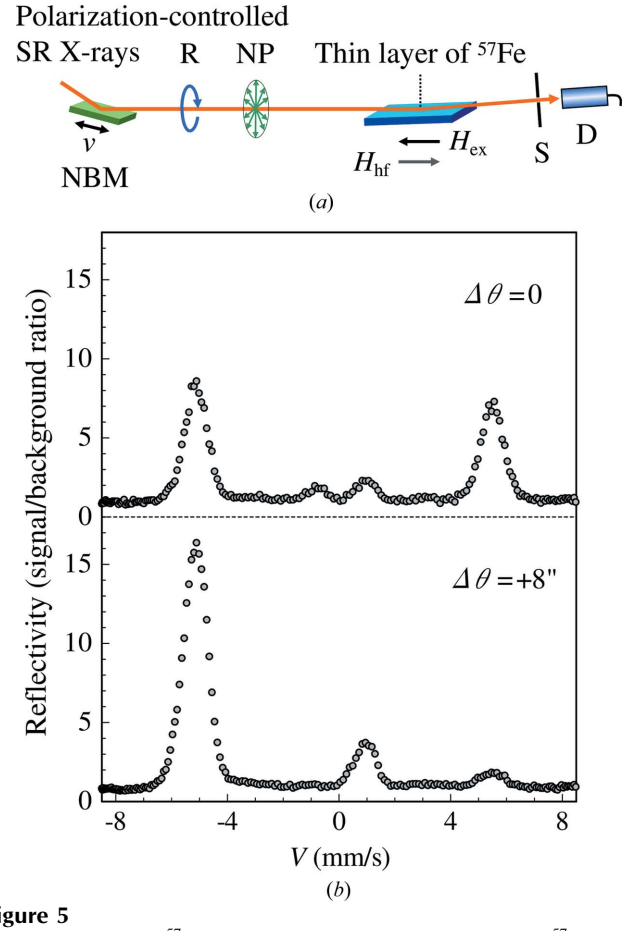

Figure 5
Grazing-incidence ^{57}Fe-SR-Mössbauer spectroscopy of a ^{57}Fe 95%-enriched ^{57}Fe(100 nm)/MgO(001) film. (*a*) Experimental set-up. NBM: nuclear Bragg monochromator; S: slit 0.5 mm (V) × 1.0 mm (H); D: NaI(Tl) detector. (*b*) Reflectivity spectra of the magnetized iron thin film at a grazing angle of 0.3°. Upper and lower parts correspond to the spectrum measured with the non-polarized and right circularly polarized ^{57}Fe-SR-Mössbauer radiation, respectively. The magnetic moment (hyperfine field) of the iron thin film has been aligned antiparallel (parallel) to the beam direction by applying an external magnetic field (H_{ex} = 600 Oe) in the film plane.

$\Delta m = +1$ nuclear transitions with full beam flux. However, in the case of the non-polarized (mixed polarization) beam incidence the $\Delta m = +1$ nuclear transitions are excited by one half of the beam flux, with right circular polarization, and the other half, with the opposite helicity, excites the $\Delta m = -1$ nuclear transitions.

In this study the developed spectrometer has been successfully applied to grazing-incidence ^{57}Fe-SR-Mössbauer spectroscopy. Polarization-controlled high-brilliance ^{57}Fe-SR-Mössbauer radiation enables the measurement of the specular nuclear resonant reflection spectrum in a short data collection time. In particular, the circularly polarized beam gives an energy-domain Mössbauer spectrum with a high signal-to-background ratio and a high sensitivity to the direction of H_{hf}. The simple optical system is very suitable for applied research under special conditions, such as low temperatures, high magnetic fields, *in situ* studies with various gas environments and non-equilibrium spin Hall conditions (Mibu *et al.*, 2015).

In the near future these advantages will give unique insights into the magnetic states at the surface and interface of various functional magnetic thin films.

6. Conclusion

A new SR-based Mössbauer spectrometer using a diamond phase plate and an iron borate nuclear Bragg monochromator has been developed at the BL11XU beamline of SPring-8. It can easily realise energy-domain ^{57}Fe-SR-Mössbauer studies with various polarization states, *i.e.* linear polarization, circular polarization and non-polarization. Its outstanding potential has been demonstrated by a grazing-incidence Mössbauer study of an iron thin film. As a special advantage the measurement is possible even in multi-bunch mode of SR. We believe that the developed spectrometer provides new possibilities for the application of polarized ^{57}Fe-SR-Mössbauer spectroscopy, including Mössbauer polarimeter (Pfannes & Gonser, 1974), γ-ray diffraction (Belyakov, 1975), ultrahigh-pressure experiments (Nasu, 1994), small-angle scattering (Shvyd'ko *et al.*, 1996) and Rayleigh scattering of ^{57}Fe-SR-Mössbauer radiation (Masuda *et al.*, 2008; Mitsui *et al.*, 2012*b*).

This work was supported by the Grants-in-Aid for Scientific Research (S) from Japan Society for the Promotion of Science (JSPS). TM and KM were partially supported by the Grants-in-Aid for Scientific Research (B) from JSPS. SR-Mössbauer studies were performed at BL11XU, SPring-8 (proposal numbers 2012A3501, 2012B3501, 2013A3501, 2013B3501, 2013B3512 and 2014A3501). The authors would like to thank Dr M. Suzuki for help with the X-ray polarization monitor.

References

Andreeva, M. A., Belozerskii, G. N., Irkaev, S. M., Semenov, V. G., Sokolov, A. Yu. & Shumilova, N. V. (1991). *Phys. Status Solidi A*, **127**, 455–464.
Andreeva, M. A., Irkaev, S. M. & Semenov, V. G. (1994). *J. Exp. Theor. Phys.* **78**, 956–965.
Batterman, B. W. & Cole, H. (1964). *Rev. Mod. Phys.* **36**, 681–717.
Belyakov, V. A. (1975). *Sov. Phys. Usp.* **18**, 267–291.
Belyakov, V. A. (1987*a*). *Usp. Fiz. Nauk.* **151**, 699–714.
Belyakov, V. A. (1987*b*). *Sov. Phys. Usp.* **30**, 331–340.
Belyakov, V. A. & Aivazyan, Y. M. (1968). *JETP Lett.* **7**, 368–370.
Belyakov, V. A. & Aivazyan, Y. M. (1969). *JETP Lett.* **9**, 393–394.
Bernstein, S. & Campbell, E. C. (1963). *Phys. Rev.* **132**, 1625–1633.
Bottyán, L., Deák, L. & Coussement, R. (2003). *SPring-8 Research Frontiers*, pp. 58–59. SPring-8, Japan.
Bouchenoire, L., Brown, S. D., Thompson, P., Duffy, J. A., Taylor, J. W. & Cooper, M. J. (2003). *J. Synchrotron Rad.* **10**, 172–176.
Bürck, U. van, Mössbauer, R. L., Smirnov, G. V. & Maurus, H. J. (1980). *J. Phys. C*, **13**, 4511–4529.
Callens, R., Coussement, R., L'abbé, C., Nasu, S., Vyvey, K., Yamada, T., Yoda, Y. & Odeurs, J. (2002). *Phys. Rev. B*, **65**, 180404.
Callens, R., L'abbé, C., Meersschaut, J., Serdons, I., Sturhahn, W. & Toellner, T. S. (2005). *Phys. Rev. B*, **72**, 081402.
Callens, R., L'abbé, C., Meersschaut, J., Serdons, I., Sturhahn, W. & Toellner, T. S. (2007). *J. Synchrotron Rad.* **14**, 366–371.
Chumakov, A. I., Niesen, L., Nagy, D. L. & Alp, E. E. (1999). *Hyperfine Interact.* **123/124**, 427–454.
Chumakov, A. I., Smirnov, G. V., Baron, A. Q. R., Arthur, J., Brown, D. E., Ruby, S. L., Brown, G. S. & Salashchenko, N. N. (1993). *Phys. Rev. Lett.* **71**, 2489–2492.
Chumakov, A. I., Zelepukhin, M. V., Smirnov, G. V., van Bürck, U., Rüffer, R., Hollatz, R., Rüter, H. & Gerdau, E. (1990). *Phys. Rev. B*, **41**, 9545–9547.
Deák, L., Bottyán, L., Callens, R., Coussement, R., Major, M., Serdons, I. & Yoda, Y. (2006). *Hyperfine Interact.* **167**, 709–715.
Finkelstein, K. D., Staffa, C. & Shen, Q. (1994). *Nucl. Instrum. Methods Phys. Res. A*, **347**, 124–127.
Frauenfelder, H., Nagle, D. E., Taylor, R. D., Cochran, D. R. F. & Visscher, W. M. (1962). *Phys. Rev.* **126**, 1065–1075.
Frost, J. C., Cowie, B. C. C., Chapman, S. N. & Marshall, J. F. (1985). *Appl. Phys. Lett.* **47**, 581–583.
Gerdau, E., Grote, M. & Röhlsberger, R. (1990). *Hyperfine Interact.* **58**, 2433–2438.
Gerdau, E. & Rüffer, R. (1986). *Hyperfine Interact.* **27**, 59–67.
Gerdau, E., Rüffer, R., Winkler, H., Tolksdorf, W., Klages, C. P. & Hannon, J. P. (1985). *Phys. Rev. Lett.* **54**, 835–838.
Gerdau, E. & van Bürck, U. (1994). *Resonant Anomalous X-ray Scattering*, edited by G. Materlik, C. J. Sparks and K. Fisher, p. 589. Amsterdam: Elsevier.
Giles, C., Malgrange, C., Goulon, J., de Bergevin, F., Vettier, C., Dartyge, E., Fontaine, A., Giorgetti, C. & Pizzini, S. (1994). *J. Appl. Cryst.* **27**, 232–240.
Gonser, U. & Fischer, H. (1981). In *Mössbauer Spectroscopy II, The Exotic Side of the Method*, edited by U. Gonser. Berlin: Springer-Verlag.
Gonser, U. & Fischer, H. (1985). *Hyperfine Interact.* **26**, 845–853.
Hannon, J. P., Hung, N. V., Trammell, G. T., Gerdau, E., Mueller, M., Rüffer, R. & Winkler, H. (1985*a*). *Phys. Rev. B*, **32**, 5068–5080.
Hannon, J. P., Hung, N. V., Trammell, G. T., Gerdau, E., Mueller, M., Rüffer, R. & Winkler, H. (1985*b*). *Phys. Rev. B*, **32**, 5081–5093.
Hannon, J. P., Trammell, G. T., Mueller, M., Gerdau, E., Rüffer, R. & Winkler, H. (1985*c*). *Phys. Rev. B*, **32**, 6363–6373.
Hannon, J. P., Trammell, G. T., Mueller, M., Gerdau, E., Rüffer, R. & Winkler, H. (1985*d*). *Phys. Rev. B*, **32**, 6374–6384.
Hannon, J. P., Trammell, G. T., Mueller, M., Gerdau, E., Winkler, H. & Rüffer, R. (1979). *Phys. Rev. Lett.* **43**, 636–639.
Hastings, J. B., Siddons, D. P., van Bürck, U., Hollatz, R. & Bergmann, U. (1991). *Phys. Rev. Lett.* **66**, 770–773.
Hayakawa, S., Ugajin, K., Sasaki, K., Miyamura, K. & Gohshi, Y. (1998). *Adv. X-ray Chem. Anal. Jpn*, **29**, 233–243. (In Japanese.)
Hirano, K., Ishikawa, T. & Kikuta, S. (1995). *Rev. Sci. Instrum.* **66**, 1604–1609.
Hirano, K., Izumi, K., Ishikawa, T., Annaka, S. & Kikuta, S. (1991). *Jpn. J. Appl. Phys.* **30**, L407–L410.
Irkaev, S. M., Andreeva, M. A., Semenov, V. G., Belozerskii, G. N. & Grishin, O. V. (1993). *Nucl. Instrum. Methods Phys. Res. B*, **74**, 545–553.
Isaenko, S. A., Chumakov, A. I. & Shinkarev, S. I. (1994). *Phys. Lett. A*, **186**, 274–278.
Jäschke, J., Rüter, H. D., Gerdau, E., Smirnov, G. V., Sturhahn, W. & Pollmann, J. (1999). *Nucl. Instrum. Methods Phys. Res. B*, **155**, 189–198.
L'abbé, C., Callens, R. & Odeurs, J. (2001). *Hyperfine Interact.* **135**, 275–294.
L'abbé, C., Coussement, R., Odeurs, J., Alp, E. E., Sturhahn, W., Toellner, T. S. & Johnson, C. (2000). *Phys. Rev. B*, **61**, 4181–4185.
L'abbé, C., Meersschaut, J., Sturhahn, W., Jiang, J. S., Toellner, T. S., Alp, E. E. & Bader, S. D. (2004). *Phys. Rev. Lett.* **93**, 037201.
Masuda, R., Mitsui, T., Kitao, S., Higashitaniguchi, S., Yoda, Y. & Seto, M. (2008). *Jpn. J. Appl. Phys.* **47**, 8087–8090.
Mibu, K., Mitsui, T., Tanaka, M., Masuda, R., Kitao, S., Kobayashi, Y., Yoda, Y. & Seto, M. (2015). *J. Appl. Phys.* In the press.

Mibu, K., Seto, M., Mitsui, T., Yoda, Y., Masuda, R., Kitao, S., Kobayashi, Y., Suharyadi, E., Tanaka, M., Tsunoda, M., Yanagihara, H. & Kita, E. (2013). *Hyperfine Interact.* **217**, 127–135.
Mirzababaev, R. M., Smirnov, G. V., Sklyarevskii, V. V., Artemev, A. N., Izrailenko, A. N. & Babkov, A. V. (1971). *Phys. Lett. A*, **37**, 441–442.
Mitsui, T., Hirao, N., Ohishi, Y., Masuda, R., Nakamura, Y., Enoki, H., Sakaki, K. & Seto, M. (2009). *J. Synchrotron Rad.* **16**, 723–729.
Mitsui, T., Kitao, S., Zhang, X. W., Marushita, M. & Seto, M. (2001). *Nucl. Instrum. Methods Phys. Res. A*, **467–468**, 1105–1108.
Mitsui, T., Masuda, R., Hirao, N., Mibu, K. & Seto, M. (2012*b*). *Hyperfine Interact.* **204**, 97–100.
Mitsui, T., Masuda, R., Seto, M., Suharyadi, E. & Mibu, K. (2012*a*). *J. Synchrotron Rad.* **19**, 198–204.
Mitsui, T., Seto, M., Kikuta, S., Hirao, N., Ohishi, Y., Takei, H., Kobayashi, Y., Kitao, S., Higashitaniguchi, S. & Masuda, R. (2007*b*). *Jpn. J. Appl. Phys.* **46**, 821–825.
Mitsui, T., Seto, M. & Masuda, R. (2007*a*). *Jpn. J. Appl. Phys.* **46**, L930–L932.
Mössbauer, R. L. (1958). *Z. Phys.* **151**, 124–143.
Nagy, D. L., Bottyán, L., Deák, L., Dekoster, J., Langouche, G., Semenov, V. G., Spiering, H. & Szilágyi, E. (1999). *Proceedings of Mössbauer Spectroscopy in Materials Science*, pp. 323–336, edited by M. Miglierini and D. Petridis. Amsterdam: Kluwer Academic.
Nagy, D. L., Bottyán, L., Deák, L., Szilágyi, E., Spiering, H., Dekoster, J. & Langouche, G. (2000). *Hyperfine Interact.* **126**, 353–361.
Nasu, S. (1994). *Hyperfine Interact.* **90**, 59–75.
Niesen, B., Mugarza, A., Rosu, M., Coehoorn, R., Jungblut, R. M., Roozeboom, F., Baron, A. Q. R., Chumakov, A. I. & Rüffer, R. (1998). *Phys. Rev. B*, **58**, 8590–8595.
Odeurs, J., Coussement, R., L'abbé, C., Neyens, G., Hoy, G. R., Alp, E. E., Sturhahn, W., Toellner, T. & Johnson, C. (1998). *Hyperfine Interact.* **113**, 455–463.
Pankhurst, Q. A., Cohen, N. S., Fernández Barquín, L., Gibbs, M. R. J. & Smirnov, G. V. (2001). *J. Non-Cryst. Solids*, **287**, 81–87.
Pfannes, H.-D. & Gonser, U. (1974). *Nucl. Instrum. Methods*, **114**, 297–299.
Planckaert, N., Callens, R., Demeter, J., Laenens, B., Meersschaut, J., Sturhahn, W., Kharlamova, S., Temst, K. & Vantomme, A. (2009). *Appl. Phys. Lett.* **94**, 224104.
Potapkin, V., Chumakov, A. I., Smirnov, G. V., Celse, J.-P., Rüffer, R., McCammon, C. & Dubrovinsky, L. (2012). *J. Synchrotron Rad.* **19**, 559–569.
Röhlsberger, R. (1999). *Hyperfine Interact.* **123/124**, 455–479.
Röhlsberger, R., Bansmann, J., Senz, V., Jonas, K. L., Bettac, A., Leupold, O., Rüffer, R., Burkel, E. & Meiwes-Broer, K. H. (2001). *Phys. Rev. Lett.* **86**, 5597–5600.
Röhlsberger, R., Gerdau, E., Lüken, E., Rüter, H. D., Metge, J. & Leupold, O. (1993). *Z. Phys. B*, **92**, 489–499.
Ruby, S. L. (1974). *J. Phys. (Paris) Colloq.* **35**, C6-209–C6-211.
Seto, M., Masuda, R., Higashitaniguchi, S., Kitao, S., Kobayashi, Y., Inaba, C., Mitsui, T. & Yoda, Y. (2009). *Phys. Rev. Lett.* **102**, 217602.
Shen, Q. (1996). *Proc. SPIE*, **2856**, 82.
Shen, Q. (2000). *Polarizing Crystal Optics*, in *Handbook of Optics*, edited by M. Bass. New York: McGraw.
Shen, Q. & Finkelstein, K. D. (1995). *Rev. Sci. Instrum.* **66**, 2374–2376.
Shen, Q., Shastri, S. & Finkelstein, K. D. (1995). *Rev. Sci. Instrum.* **66**, 1610–1613.
Shiwaku, H., Mitsui, T., Tozawa, K., Kiriyama, K., Harami, T. & Mochizuki, T. (2004). *AIP Conf. Proc.* **705**, 659–662.
Shtrikman, S. (1967). *Solid State Commun.* **5**, 701–703.
Shtrikman, S. & Somekh, S. (1969). *Rev. Sci. Instrum.* **40**, 1151–1153.
Shvyd'ko, Yu. V., Chumakov, A. I., Baron, A. Q. R., Gerdau, E., Rüffer, R., Bernhard, A. & Metge, J. (1996). *Phys. Rev. B*, **54**, 14942–14945.
Siddons, D. P., Bergmann, U. & Hastings, J. B. (1999). *Hyperfine Interact.* **123/124**, 681–719.
Siddons, D. P., Hart, M., Amemiya, Y. & Hastings, J. B. (1990). *Phys. Rev. Lett.* **64**, 1967–1970.
Siddons, D. P., Hastings, J. B., Faigel, G., Berman, L. E., Haustein, P. E. & Grover, J. R. (1989). *Phys. Rev. Lett.* **62**, 1384–1387.
Smirnov, G. V. (1996). *Hyperfine Interact.* **97/98**, 551–588.
Smirnov, G. V. (2000). *Hyperfine Interact.* **125**, 91–112.
Smirnov, G. V., Chumakov, A. I., Potapkin, V. B., Rüffer, R. & Popov, S. L. (2011). *Phys. Rev. A*, **84**, 053851.
Smirnov, G. V., Sklyarevskii, V. V., Voscanian, R. A. & Artemev, A. N. (1969). *JETP Lett.* **9**, 70–73.
Smirnov, G. V., van Bürck, U., Chumakov, A. I., Baron, A. Q. R. & Rüffer, R. (1997). *Phys. Rev. B*, **55**, 5811–5815.
Smirnov, G. V., Zelepukhin, M. V. & van Bürck, U. (1986). *JETP Lett.* **43**, 352–355.
Sturhahn, W., L'abbé, C. & Toellner, T. S. (2004). *Europhys. Lett.* **66**, 506–512.
Suzuki, M. (2004). PhD thesis, University of Tokyo, Japan. (In Japanese.) (downloadable from http://repository.dl.itc.u-tokyo.ac.jp/dspace/handle/2261/49040.)
Szymański, K. (2006). *Phys. Rep.* **423**, 295–338.
Szymański, K., Dobrzyński, L., Prus, B. & Cooper, M. J. (1996). *Nucl. Instrum. Methods Phys. Res. B*, **119**, 438–441.
Toellner, T. S., Sturhahn, W., Röhlsberger, R., Alp, E. E., Sowers, C. H. & Fullerton, E. E. (1995). *Phys. Rev. Lett.* **74**, 3475–3478.
Trammell, G. T. (1961). *Proc. Int. At. Energ. Agency Symp. Chem. Eff. Nucl. Transformations*, **1**, 75–84.
Ueji, Y., Bisaiji, Y., Kuriyama, T., Okitsu, K. & Amemiya, Y. (2005). *Acta Cryst.* A**61**, C433.
Wagner, F. E. (1968). *Z. Phys.* **210**, 361–379.
Zhan, Q. F., Vandezande, S., Temst, K. & Van Haesendonck, C. (2009). *New J. Phys.* **11**, 063003.